

Article

Virtual Prototyping of Bulk Material Preparation Devices in Mining Using Multiphysics Simulations

Jarosław Tokarczyk ^{*}, Daniel Kowol , Kamil Szewerda  and Piotr Matusiak 

KOMAG Institute of Mining Technology, Pszczyńska 37, 44-101 Gliwice, Poland; dkowol@komag.eu (D.K.); kszewerda@komag.eu (K.S.); pmatusiak@komag.eu (P.M.)

^{*} Correspondence: jtokarczyk@komag.eu

Abstract: This paper presents the process of virtual prototyping of bulk material preparation devices in mining using numerical simulations of multi-physics phenomena. The discrete element method (DEM), meshless method (MFree), and computational fluid dynamics (CFD) were used in the calculation process. The importance of the extraction process and the practical application of DEM in various industries are discussed. The main contact models between particles and how structural material wear is modelled in DEM are presented. The structure of the computational models in DEM and CFD environments is presented. For the validation of the bulk material computational model, bench tests were carried out to determine the material properties (aggregate: five grades, 0–16 mm; coal concentrate: five grades, 2–32 mm; and so-called raw coal, grade 2–8 mm). The bulk density and angle of natural repose were measured, along with determination of the internal and external friction coefficients. Simulations corresponding to the laboratory tests were carried out. Numerical calculations were carried out for the side chute (results—velocities of the particles, compressive forces in the particles, determination of the wearing process) and for the coke classification line (two lines were assessed according to different aggregate sizes and densities of the bulk material). These multi-physics calculations required a combination of DEM-MFree and DEM-CFD methods. Based on the obtained results, it was possible to evaluate the performance and efficiency of the assessed machines.

Keywords: discrete element method; aggregate; co-simulation; coal preparation; computational fluid dynamics



Citation: Tokarczyk, J.; Kowol, D.; Szewerda, K.; Matusiak, P. Virtual Prototyping of Bulk Material Preparation Devices in Mining Using Multiphysics Simulations. *Appl. Sci.* **2024**, *14*, 5903. <https://doi.org/10.3390/app14135903>

Academic Editor: Fernando Rocha

Received: 10 June 2024

Revised: 3 July 2024

Accepted: 4 July 2024

Published: 5 July 2024



Copyright: © 2024 by the authors. Licensee MDPI, Basel, Switzerland. This article is an open access article distributed under the terms and conditions of the Creative Commons Attribution (CC BY) license (<https://creativecommons.org/licenses/by/4.0/>).

1. Introduction

Computer-aided designing has been utilized for many decades. Most often, it concerns strength calculations using the finite element method (FEM). However, due to the constant increase in the computing power of computers and the continuous development of software environments that enable the simulation of many physical phenomena, it becomes possible to create computational tasks combining the discrete element method (DEM), computer fluid dynamics (CFD), and the meshless method (MFree). The use of many numerical methods makes it easier to optimize a design of a given solution in relation to many evaluation criteria. Simulations using DEM support the design and manufacturing process of new solutions for machine components that are used in various industries, including technological processes and/or for the transport of bulk materials. The support consists of calculating static and dynamic loads from the transported bulk material, affecting the structural components (parts, subassemblies) exposed to direct contact with the moving material; estimating the wear of components exposed to direct contact with the bulk material, e.g., during its transport; assessment of the efficiency and effectiveness of sorting machines and screens at the stage of their designing and manufacturing as well as selection of the process control algorithms in technological lines.

1.1. Mining Industry

The mining industry is a key source of raw materials for other industries. For example, coal mining is necessary to produce electricity and heat. Oil extraction is also crucial for the production of fuels, plastics, and many other products. The mining industry also provides raw materials for the production of metals such as gold, silver, and copper, which are used in electronics, construction, and many other industries [1,2].

The products of the mining industry (mineral raw materials) are divided into the following groups:

- Metallic: ferrous (e.g., iron ore, manganese, nickel, cobalt); non-ferrous (e.g., copper, lead, tin, bauxite); precious metals (e.g., gold, silver, platinum);
- Non-metallic (e.g., rock salt, potassium salt, sulfur, granite, marble, limestone, aggregates);
- Mineral raw materials for energy production (hard coal, brown coal, crude oil, natural gas) [3].

The extracted raw mineral is a mixture of grains of various sizes and shapes and with different mineral compositions. The material in this form is usually not suitable for direct use; therefore, it should be subjected to processing to obtain optimal and acceptable commercial parameters [4]. The analysis of the volume of mineral resource extraction indicates significant potential for the development of the machines and equipment intended for the processing of the above-mentioned materials. For example, iron ore production in 2023 amounted to 2398.3 million tons, and the main shareholders were Brazil, China, Russia, India, and Australia [5,6]. In turn, the total global production of manganese in 2021 was 49.5 million tons, and the largest producer in the world was South Africa [7]. The highest extraction volume is the case of sand and gravel. According to online sources and UN analyses, 50 billion tons of these materials are mined every year [8].

In mechanical processing, the task of which is to separate the cleanest possible useful grains from the raw material and the cleanest waste grains devoid of a useful component, three basic operations can be distinguished [4]: classification—as a result of which the material is separated into groups of grains with specific dimensions; beneficiation—the aim of which is to divide the material into groups of grains with the same mineral characteristics; crushing—reducing the size (breaking into smaller parts) of the grains.

Dimensional classification of raw minerals mostly uses screening machines. These devices are used in the processing the raw minerals at many stages of the technological process, not only for the dimensional classification of raw material but also for the dewatering of some beneficiation products, as well as the dimensional classification of final (commercial) products.

Screening machines play a significant role in iron ore processing, which is why various types of the above devices are available on the market [9–11]. Screeners are one of the main machines used in aggregate processing. Much of this material is subjected to preparatory operations before its use, including dimensional classification. There is a very large number of companies that have their devices available for this purpose [12–14]. Screeners are also very often used in the hard coal mining industry, and even in the metallurgical industry (coke screening) [15–17]. Another example shows that screens are also important in the processing of salt rocks [18].

In the case of the second main operation of minerals processing, i.e., beneficiation, water pulsating jigs, using the phenomenon of the density separation of particles, are the devices most commonly used. Separation takes place in a pulsating water stream based on differences in the settling rates of the grains being beneficiated. Water pulsating jigs are the devices commonly used in hard coal beneficiation [19–23] and washing the aggregates [24,25]. Important areas of jig application include iron ore [26–29] and manganese ore [30,31]. Jig beneficiation is also available for alluvial gold concentration, tungsten ore pre-densification, washing the phosphate ores, and concentration of tin and copper ores [32]. Such a wide range of use of these tools in mineral mechanical processing, combined with the volume of their production and the constantly increasing demand for these

minerals, forms the basis for research work to increase the effectiveness and reliability of the above-mentioned devices.

1.2. Practical Usage of DEM

According to [33], the DEM method has been used in mineral mining and processing since the 1990s. This method is used, among others, to analyze processes related to the transport of excavated materials, crushing, screening, and flotation. One example of the use of the DEM method is the analysis of particle movement on banana flip-flow screens. Understanding the characteristics of particle vibrations contributes to optimizing the technological processes, e.g., via proper generation of vibrations (linear, clockwise, or counterclockwise), as well as the optimal selection of the vibration frequency and amplitude. Inclination of the sieves is also analyzed in the simulation process. As a result of such analyses, the efficiency of machines increases, ensuring the optimal operation [34,35]. The application of DEM simulations in the screening process is also presented in [36]. In this article, the authors analyzed the method of separating the particles of the sieved material under the impact of vibrations. Analysis of the inertial operation of a cone crusher is another example of using DEM. In [37], in order to optimize the machine's operation and with the aim of reducing the wear intensity of the linings and reducing production costs, the authors decided to carry out the parallel simulations by combining DEM simulations with a crusher model built in the environment for analyzing the systems kinematics and dynamics of multi-body systems (MBS).

Another application of co-simulation is the wet vertical stirred media mill model. The aim of the simulation was to predict the wear of each part of the mill, predict energy consumption, and learn the dynamics of both the grinding fluid and the grinding media. The authors in the article [38] presented a computational model consisting of three parts: the first part was a model of the mill structure that was created in a software environment based on FEM; the second part of the computational model was the grinding fluid model, which was modelled using the particle finite element method (PFEM); the last part of the model was the grinding medium model, which was developed in a program based on the DEM. Weak two-way couplings were defined between each model. The distribution of forces was defined by the resistance coefficient as a function of the Reynolds number. A similar approach to co-simulation was described in [39]. In this case, DEM, combined with the method of dynamics of multi-body systems and a novel particle replacement model (PRM), was used to analyze the pellet grinding process and simulate the effectiveness of high-pressure grinding rolls (HPGR). In this case, crushing was not only aimed at reducing the size of the lumps of run-of-mine, but it was also important from the point of view of releasing valuable components from the extracted ore. For a more detailed understanding of the crushing process along with the analysis of interfacial cracking, DEM simulations can also be used. This problem was presented by the authors in [40]. The analysis and development of copper ore crushing processes in hammer crushers, using co-simulation of DEM and PRM methods, was also dealt with in [41]. Another example of using DEM simulations to analyze crushing processes is presented in [42]. The presented simulations performed a comprehensive analysis of the loads in the mantle, the crushing torque, and crushing power in relation to a mining gyratory crusher operating in a copper mine.

The process opposite to the crushing process is the granulation process, i.e., combining small particles into larger ones. This is a much more complicated phenomenon than the crushing process. During the technological process, as a result of mixing, movement, or vibration, granulation and crushing of the larger particles may occur at the same time. This phenomenon depends on many physical parameters of the material. The use of DEM simulations to analyze granulation processes is presented in [43]. Another field of application of the DEM is the prediction of wear of the machine components as a result of their operation. The wear of a mining rope shovel bucket analysis presented in [44] is an example of an analysis carried out for this purpose. Based on the results of numerical simulations, it is possible to learn more about how the excavator bucket wears

in friction, both regarding the wear location and its size. An analysis of the results allows for planning maintenance and repair work, and it also directs work to optimize the bucket design. Another aspect of using DEM simulations is the possibility of simulating the cooperation of machines during the technological process. An analysis of cooperation of a longwall shearer with the armored face conveyor (AFC) described in [45] is an example of such an application of numerical simulations in mining operations. The author paid special attention to the aspect of loading the excavated material onto the longwall conveyor with changing kinematic parameters of the longwall shearer's movement. The aim of the simulation was to optimize the cooperation of both machines and avoid emergency situations, such as burying the AFC, resulting in it getting stuck. DEM is also used on a smaller scale, namely, to optimize the cutting tools used in the mining machines. For this purpose, it is required to understand the interaction between the tool and the rock in the mining process. This issue was presented in [46], where the authors discussed simulations enabling the analysis of the rock cracking mechanism.

In turn, [47] presents the possibility of using the DEM simulation method to analyze the deformation of roof rocks in mining areas. By analyzing stresses, places of stress accumulation, and geological conditions, the authors drew attention to the threats, e.g., water, occurring in a given region. By thoroughly understanding the nature of the phenomenon, the occurrence of selected hazards in the mine can be minimized.

The mining industry is one of the most important sources of income in many countries, as the development of the mining industry often regulates the source of potential and economic growth of countries [48]. The mining industry includes the exploration, planning, and permissions for the building of mines, extraction of raw minerals in open-pit and/or underground mines, processing of minerals, and recultivation of mine areas at the end of their economic life [1].

2. Materials and Methods

The DEM [49] is intended to simulate the motion of many elements (particles) of finite dimensions. As defined by [50], computer programs using the DEM should enable simulations of the finite displacements and rotations of discrete bodies (including the possibility of their complete detachment from each other) and automatically detect all interactions (contacts) among the elements in the simulation process. In the DEM, discrete elements are assumed to be rigid particles of a given mass that can move independently of each other, both in sliding movement and rotation.

2.1. Contact Models

Particles interact with each other through the so-called contact models that describe mutual acting forces and force moments. Changes in the state of the system over time are calculated numerically using the so-called explicit integration methods. The forces acting on the system may lead to static equilibrium (in which there is no particles movement) or cause the flow of bulk material (particle movement). If the contact model is assumed, describing the elastic interaction between particles, their mutual behavior uses the so-called "soft contact", in which a specific set stiffness of a particle in the normal direction describes the contact force of the connection between the adjacent particles. As a result, each particle may overlap with each other near the contact point, reflecting the compressibility of the material. In software tools based on DEM, it is possible to define various contact models that reflect the types of physical interactions between molecules [51]. The following contact models should be mentioned here:

- Hertz–Mindlin (no slip)—the default model due to its accurate and efficient calculation of force values. In this model, the normal component of the force is based on Hertz's contact theory [52]. The tangential force model is based on the work of Mindlin–Deresiewicz [53,54]. Both normal and tangential forces have damping components, where the damping coefficient is related to the coefficient of restitution, which is discussed in [55]. The tangential friction force follows the model of Coulomb's friction

law [56]. Rolling friction is implemented as a contact-independent directional constant torque model [57].

- Hertz–Mindlin with JKR (Johnson–Kendall–Roberts)—cohesive contact model that takes into account the impact of Van der Waals forces in the contact zone and allows for modelling of highly adhesive systems such as dry powders or wet materials. In this model, implementation of the normal elastic contact force is based on the Johnson–Kendall–Roberts theory [58].
- Hysteretic spring contact—taking into account plastic deformations in the contact mechanics equations, as a result of which the particles behave elastically up to a predefined stress. Once this stress is exceeded, the particles behave as if they were undergoing plastic deformation. As a result, it is possible to obtain large contact surfaces between particles without excessive forces acting on them, which represents a compressible material. The calculation of the normal force is based on the Walton–Braun theory, presented in [59,60].
- Damped linear spring compression force model, based on the work of [56]. A linear spring with stiffness k is connected in parallel with a damper with coefficient c .
- EEPA elastic–plastic adhesion model (Edinburgh Elasto-Plastic Adhesion Model)—takes into account the dependence of past interactions, which is crucial, and the characteristic behaviors of cohesive solids. The flow behavior and transfer characteristics of cohesive granular solids are strongly dependent on the prior consolidation stress in the given body. The contact model includes a nonlinear spring model with hysteresis, which takes into account the elastic–plastic contact deformation and the adhesion force component. It has been assumed that the peel force (adhesion) increases with an increase in the plastic contact area [61,62].

Moreover, particles can be combined into groups to create more complex and larger granular structures; for example, rocks and stones. Taking into account the heterogeneity of grains (different particle sizes) and the presence of internal cracks (through the appropriate distribution of the parameters of permanent connections), the material crushing process can be simulated. This movement is the result of external forces and contact forces between adjacent particles and between particles and external space constraints, e.g., vessel walls. In the DEM, the selection of the time step size results from the assumption that, in a single step, the structure disturbance will not propagate further than between immediately adjacent particles.

2.2. Models of Constructional Materials Wear

The DEM enables simulations of abrasive or erosive wear processes that cause degradation of the material surface of the structure in contact with the bulk material. There are several main material consumption models.

2.2.1. Relative Wear

Relative wear is the basic model for predicting material wear. It allows for a determination of the main areas where wear occurs and its intensity. The contact energy is calculated to estimate the spatial distribution of wear. The tool should be considered as a qualitative assessment of wear, without quantifying the depth of wear. There is a linear relationship between contact energy and wear. The values are calculated using the following formulas and spatial relationships (Figure 1):

$$E_n = \sum F_n v_n \delta_t \quad (1)$$

$$E_t = F_t v_t \delta_t \quad (2)$$

where:

- E_n —accumulated contact energy in the normal direction to the contact surface [J];
- E_t —accumulated contact energy in the tangential direction to the contact surface [J];
- F_n —contact force in the direction normal to the contact surface [N];

- F_t —contact force in the direction tangential to the contact surface [N];
- v_n —speed of the particle in the direction normal to the contact surface [m/s];
- v_t —speed of the particle in the direction tangential to the contact surface [m/s];
- δ_t —integration step [s].

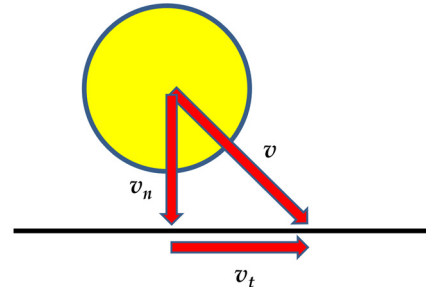


Figure 1. System of significant vectors in the relative wear model.

2.2.2. Abrasive Wear

Archard's model [63] enables the calculation of the amount of material removed from the surface as a result of the abrasion process. This model requires calibration based on empirical data. As a result of the calculations, it is possible to obtain surface deformations in the computational model. The Archard model describes the linear relationship between the normal force and the wear volume between the moving particle and the degraded surface. Its basic formulas and spatial relationships are given in Figure 2.

$$d_w = \frac{E}{A} \quad (3)$$

$$E = \frac{K}{H_v} F_n \Delta U \quad (4)$$

where:

- d_w —wear depth [m];
- E —wear volume [m³];
- A —surface area of the penetrated surface element [m²];
- K —empiric constant;
- H_v —hardness of the used material acc. to Vickers scale [GPa];
- F_n —contact force in the direction normal to the contact surface [N];
- ΔU —distance travelled by a particle while contacting the surface [m].

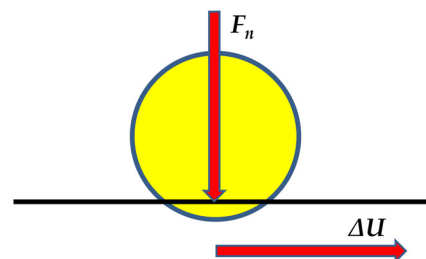


Figure 2. System of significant vectors in the abrasive wear model acc. to Archard.

2.2.3. Oka Wear Model

Using the Oka model [64,65], it is possible to calculate the depth of material loss from the surface of the contact element as a result of erosive wear (due to the impact of each

particle). The model requires calibration (empirical tests). The following formulas and spatial relationships are used in the Oka model (Figure 3).

$$\frac{E(\alpha)m_p}{A} \quad (5)$$

$$E(\alpha) = 65W^{-k_1} \left(\frac{v}{104} \right)^{2.3H_v^{0.038}} \left(\frac{D}{0.326} \right)^{0.19} \quad (6)$$

$$g(\alpha) = \sin(\alpha)^{0.71H_v^{0.14}} [1 + H_v(1 - \sin(\alpha))]^{2.4H_v^{-0.94}} \quad (7)$$

where:

- d_w —depth of erosion loss [mm];
- $E(\alpha)$ —unit loss volume [mm³/kg];
- $g(\alpha)$ —dependence of the impact angle on standardized erosion;
- A —surface area of the penetrated surface element [m²];
- m_p —particle mass [kg];
- α —angle of direction from which a given particle hits [rad];
- v —speed of the particle when it hits the surface [m/s];
- D —particle diameter [mm];
- H_v —hardness of the used material acc. to Vickers scale [GPa];
- W —material erosion wear constant. The constant takes the following values [64]: carbon steel: $W_{Oka} \sim 3$; stainless steel: $W_{Oka} \sim 10$; aluminum: $W_{Oka} \sim 1000$.

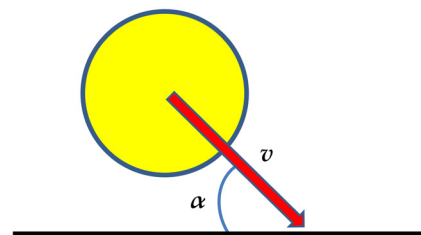


Figure 3. Significant vector system in the Oka model of abrasive wear.

2.3. Algorithm of Creating the Computational Task

In the DEM, creation of the computational tasks begins with defining the bulk material model. This model is created based on appropriate input data, including the bulk density, angle of natural repose, internal friction coefficient, and external friction coefficient. At the same time, a spatial geometric model of the object is introduced into the software environment, which limits or directs the flow of the bulk material. Boundary conditions and material properties are then defined. After the calculations, it is possible to obtain the calculation results for the particles and for the object in which they are located or which limits their movement (Figure 4).

The results obtained for the DEM-based simulation can be used to assess the object strength. For this purpose, the contact force field is saved as an external file and imported into a program environment based on the FEM or MFree methods. Then, after completion of the computational model with material properties and boundary conditions, numerical calculations are performed, based on which results such as in the “typical” finite element method, i.e., stresses, strains, displacements, and reaction values, are obtained.

Computational tasks created in the DEM software environment can take into account fluid flow phenomena. For this purpose, the co-simulation mode is used, i.e., programs based on DEM and CFD methods exchange specific data at each iteration step. The development of a CFD computational model requires the creation of a geometric model of the fluid domain, the selection of analysis taking into account the time parameter (transient analysis), the type of flow (laminar or turbulent), the definition of the particle

carrier material model (liquid or gas), and the determination of the initial and boundary conditions (Figure 5).

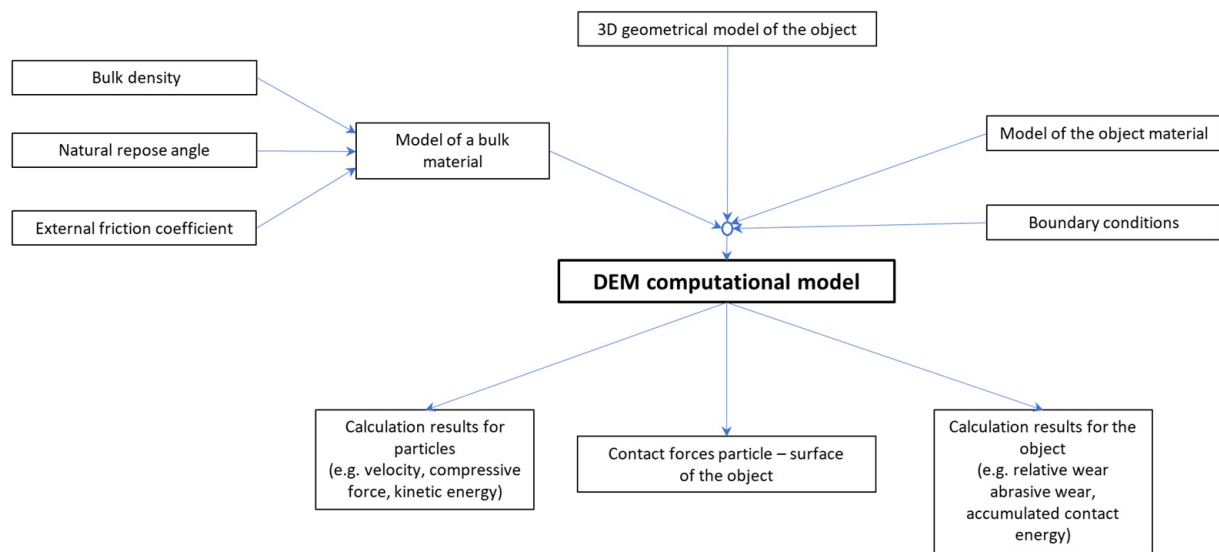


Figure 4. Creation of the computational task based on the DEM.

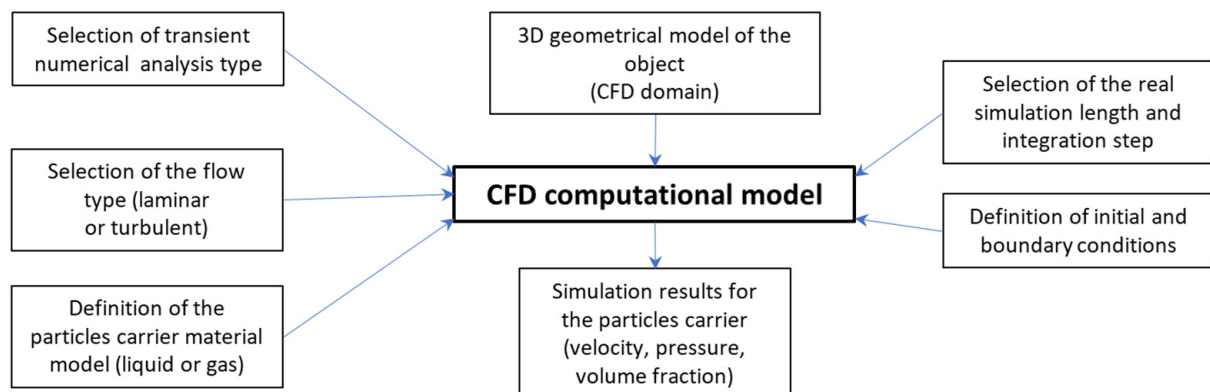


Figure 5. Creation of the computational task based on CFD.

3. Implementation of the Method

In the examples, the DEM–MFree methods were used to analyze the strength of a side chute, while the co-simulation of the DEM–CFD methods was presented in the assessment of the output of a section of the coking coal classification line. Both devices are used in mining processing plants.

3.1. Defining the Bulk Material Model

Aggregate is a material that is usually of organic or mineral origin and is mainly used for the production of building mortars, concrete, and for road construction. Aggregates are divided according to their method of extraction. There are natural and artificial aggregates. Natural aggregates come from minerals crushed by rock erosion or are obtained mechanically by crushing the solid rocks. This type of aggregate can be refined through screening and washing/beneficiation processes. Natural aggregates are divided into gravel and crushed aggregates. Artificial aggregates include those of mineral origin, obtained as a result of thermal or other modifications, and recycled aggregates, obtained as a result of the processing of inorganic materials previously used in construction. The use of aggregates depends on a number of factors (parameters), including mechanical strength, frost resistance, water absorption, and chemical and grain composition. Aggregates are

used in construction (including concrete production, road surfaces, backfilling industry), railways (substructures for railway tracks, railway embankments), the glass industry (use of quartz sand of very fine granulation), foundry (use of foundry sands with very high quartz contents), water and sewage filtration (purification plants and home water filters), the electronics industry (use of sands with very high quartz contents), and the mining industry (use of aggregates for the extraction of hydrocarbons using hydraulic fracturing), as well as for decoration.

For the purposes of numerical simulations, stand tests were carried out to determine the properties of an aggregate, coal concentrate, and the so-called raw coal. The bulk density and angle of natural repose were measured, along with determinations of the coefficient of internal friction and the coefficient of external friction. For each type of material, three tests were performed, and the results of each were recorded. Based on the recorded results, the average value of each parameter was calculated. The average values of the external friction coefficient of the selected bulk materials in relation to polished and typical steel are presented in Table 1.

Table 1. External friction coefficient for the selected bulk materials.

Surface Type	Material Type	Average Value of the Minimum Slide Angle (°)	Friction Coefficient
Polished steel	Aggregate, 0–0.5 mm	22	0.40
	Aggregate, 1–2 mm	21	0.38
	Aggregate, 2–4 mm	20.3	0.37
	Aggregate, 6–8 mm	20	0.36
	Aggregate, 8–16 mm	21	0.38
	Coal concentrate, 2–4 mm	25.3	0.47
	Coal concentrate, 8–16 mm	24.7	0.46
	Coal concentrate, 16–32 mm	26.7	0.46
	Raw coal, 2–8 mm	22.3	0.41
Typical steel	Aggregate, 0–0.5 mm	23	0.42
	Aggregate, 1–2 mm	22.3	0.41
	Aggregate, 2–4 mm	22.7	0.42
	Aggregate, 6–8 mm	25	0.47
	Aggregate, 8–16 mm	26.3	0.49
	Coal concentrate, 2–4 mm	26.7	0.50
	Coal concentrate, 8–16 mm	28	0.53
	Coal concentrate, 16–32 mm	26.3	0.49
	Raw coal, 2–8 mm	23.7	0.44

The article further presents the method for the computational model of bulk material validation in relation to 16–32 mm coal concentrate. A similar procedure applies to other types and assortments of bulk materials. Based on the stand tests, the following properties of the bulk material were defined: bulk density: $<1000 \text{ kg/m}^3$; natural repose angle: 35.5° ; JKR: 0; coefficient of restitution COR: 0.5; stiction coefficient (static friction): 1.0; rolling friction coefficient: 0.15; material density: 1600 kg/m^3 ; static friction coefficient of the substrate: 0.49.

The following particle parameters were determined: spheres—particles consisted of three spheres, each with a radius of 9.5 mm (Figure 6), and particle dimensions—to take into account the dimensional range of the aggregate, a random distribution of particle dimensions from 0.85 to 1.00 of its nominal size, i.e., 32 mm, was introduced.

To obtain the correct results, i.e., compliance regarding the natural angle of repose, the iterative method was used. This involved determining the initial particle parameters, determining the substrate parameters, and calculating and measuring the angle of repose obtained from the calculations. If there were differences, corrections were made for the geometric features and particle density. These were repeated many times until the angle of repose results were within the tolerance of $\pm 0.5^\circ$. When displaying the results, it is

possible to visualize particles using the so-called templates of geometric forms. Figure 7 shows sample templates of geometric shapes and the final effects of their use, assuming that the remaining parameters of the bulk material remain unchanged.

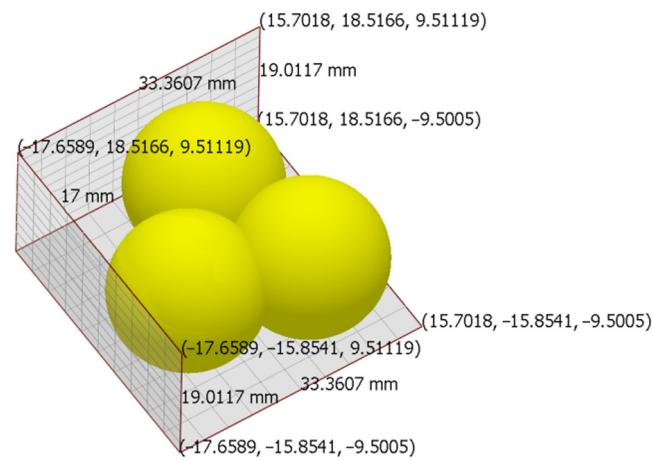


Figure 6. View of a particle representing a 16–32 mm coal concentrate in the EDEM program.

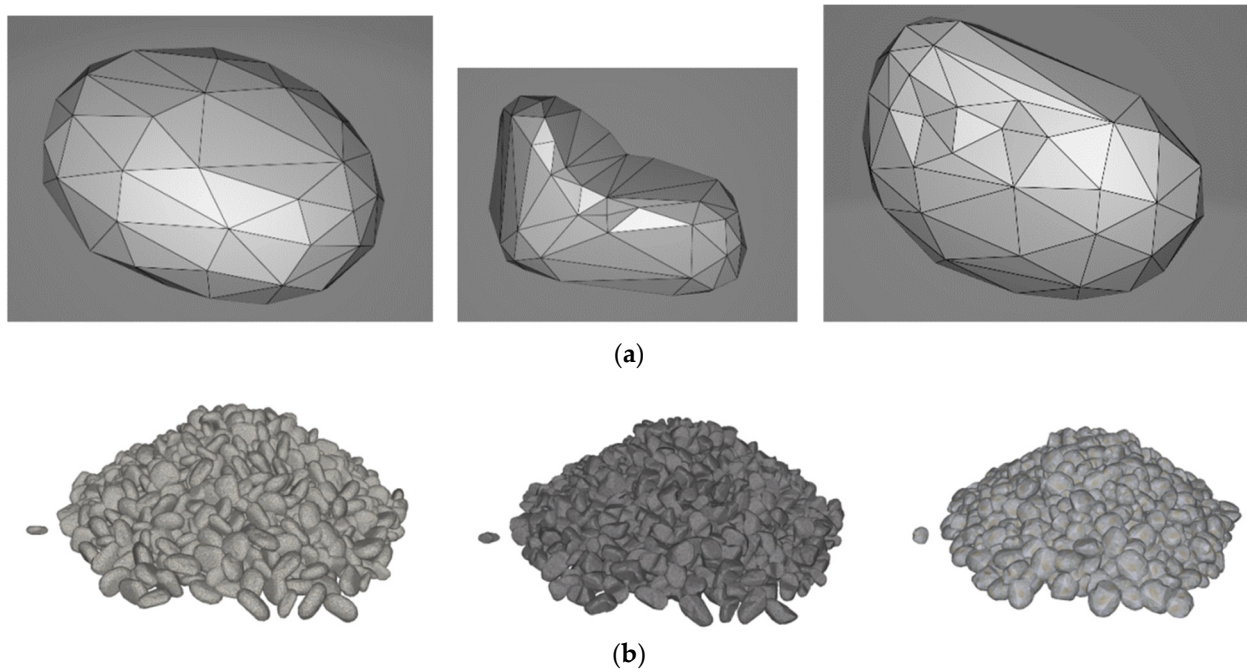


Figure 7. View of the template of the geometric form of bulk material (a) and the result of their application in the DEM results (b).

The conditions prevailing at the test stand were recreated in a DEM-based software environment, i.e., the formation of a bulk cone as a result of emptying the bottomless vessel was simulated (Figure 8).

The following particle parameters were determined: spheres—particles consisted of three spheres, each with a radius of 9.5 mm (Figure 6); particle dimensions—to take into account the dimensional range of the aggregate, a random distribution of particle dimensions from 0.85 to 1.00 of its nominal size, i.e., 32 mm, was introduced.

After completing the simulation of the of the bulk material cone formation, its target form was obtained. Figure 9 shows the cone without a template, using a template, and its form obtained on the basis of stand tests.

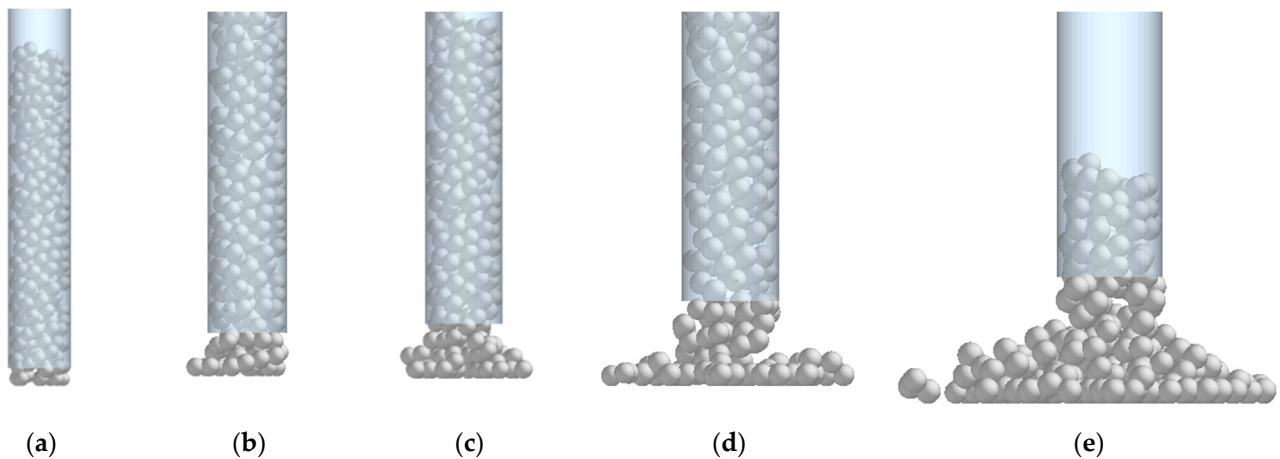


Figure 8. Movement of the laboratory vessel upwards with formation of a bulk cone: $t = 1.20$ s (a), $t = 2.0$ s (b), $t = 2.5$ s (c), $t = 3.0$ s (d); $t = 4.0$ s (e).

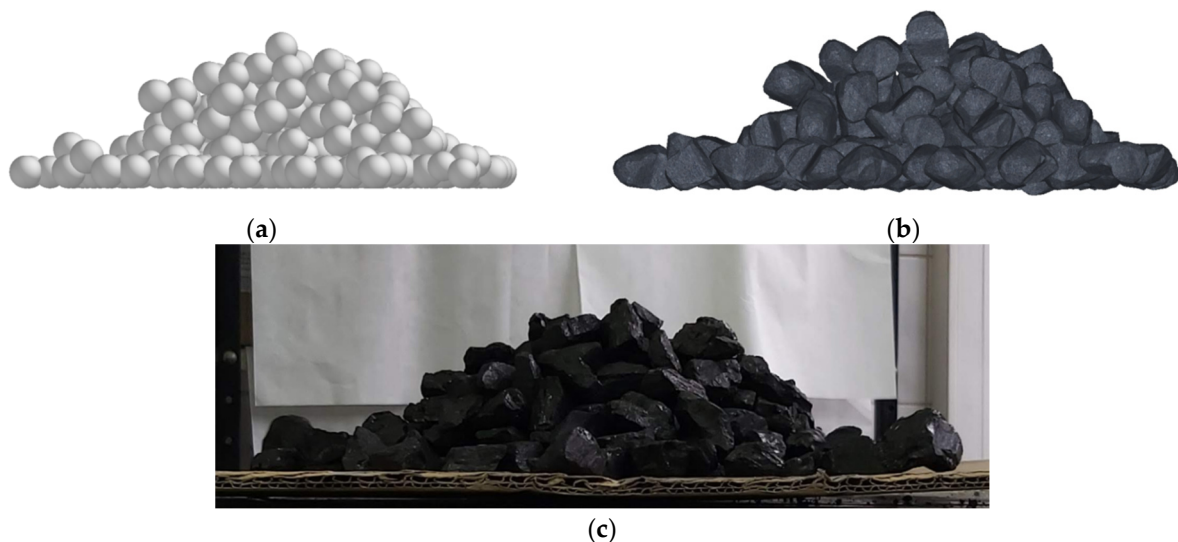


Figure 9. View of the bulk cone for coal concentrate 16–32 mm: DEM simulation without using a template (a), DEM simulation using a template (b), stand tests (c).

After validation, the bulk material model was part of the DEM computational models, which were used to assess the side chute and part of the coke classification line.

3.2. Side Chute

Side chutes are designed for loading railway wagons in hard coal mines. They are installed at the side outlets from the tanks for the backfilling of fine stones for waste in the form of filter cakes on wagons. These are welded sheet metal structures made of structural steel. The bottom of the chute and the side walls are exposed to intensive abrasion with the transported material. To facilitate transport and assembly, the chute has a modular design. The 3D geometrical model of the side chute was simplified by removing holes, standardized fasteners (screws, washers, nuts), and driving components (pneumatic cylinder). Figure 10 shows the spatial geometrical model of the chute before and after the simplifications.

The following material properties of the chute's structural elements were assumed: Poisson's number (ν)—0.3; density (ρ)—7800 kg/m³; Young's modulus (E)— 2.6×10^8 Pa; coefficient of restitution—0.35; static and kinetic friction coefficients—0.2; hardness acc. to Vickers scale H_V —10.8 GPa. The chute capacity was assumed to be 50 kg/s for the 16–32 mm material. Figure 11 shows the selected results of the DEM simulation for particles of the bulk material and for the chute's constructional material (Figure 12).

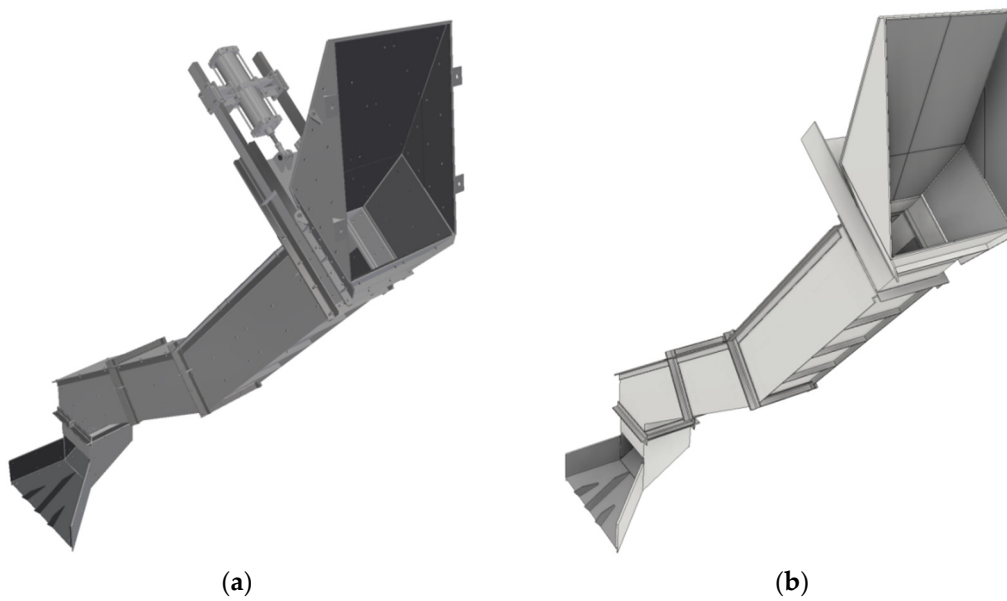


Figure 10. 3D geometrical model of the side chute: designed model (a), simplified model (b).

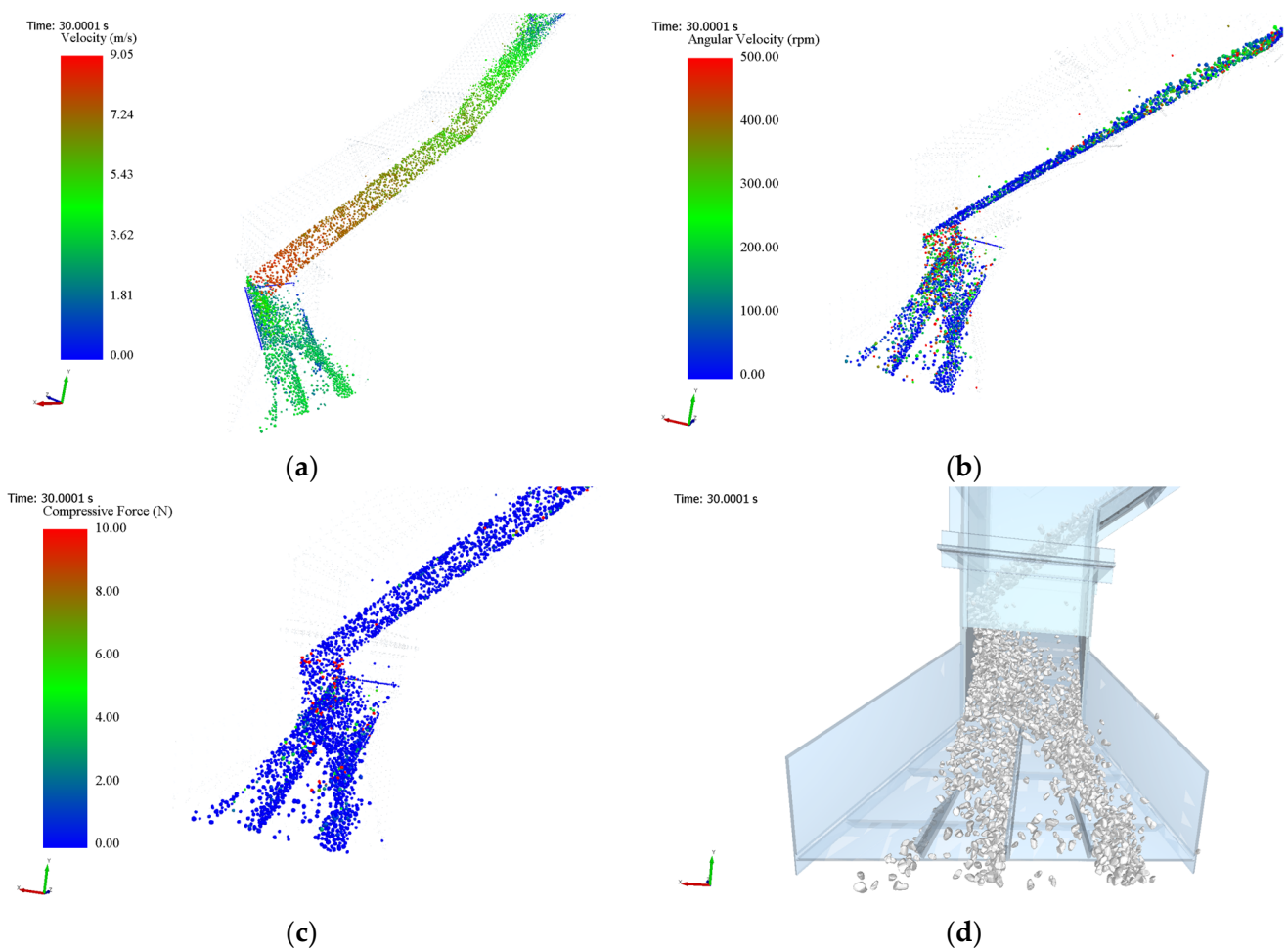


Figure 11. Calculation results for bulk material in the side chute: linear velocity of particles (a); angular velocity of particles (b); compressive forces in particles (c); general view of aggregate particles using a template for visualization in the area of the chute outlet (d).

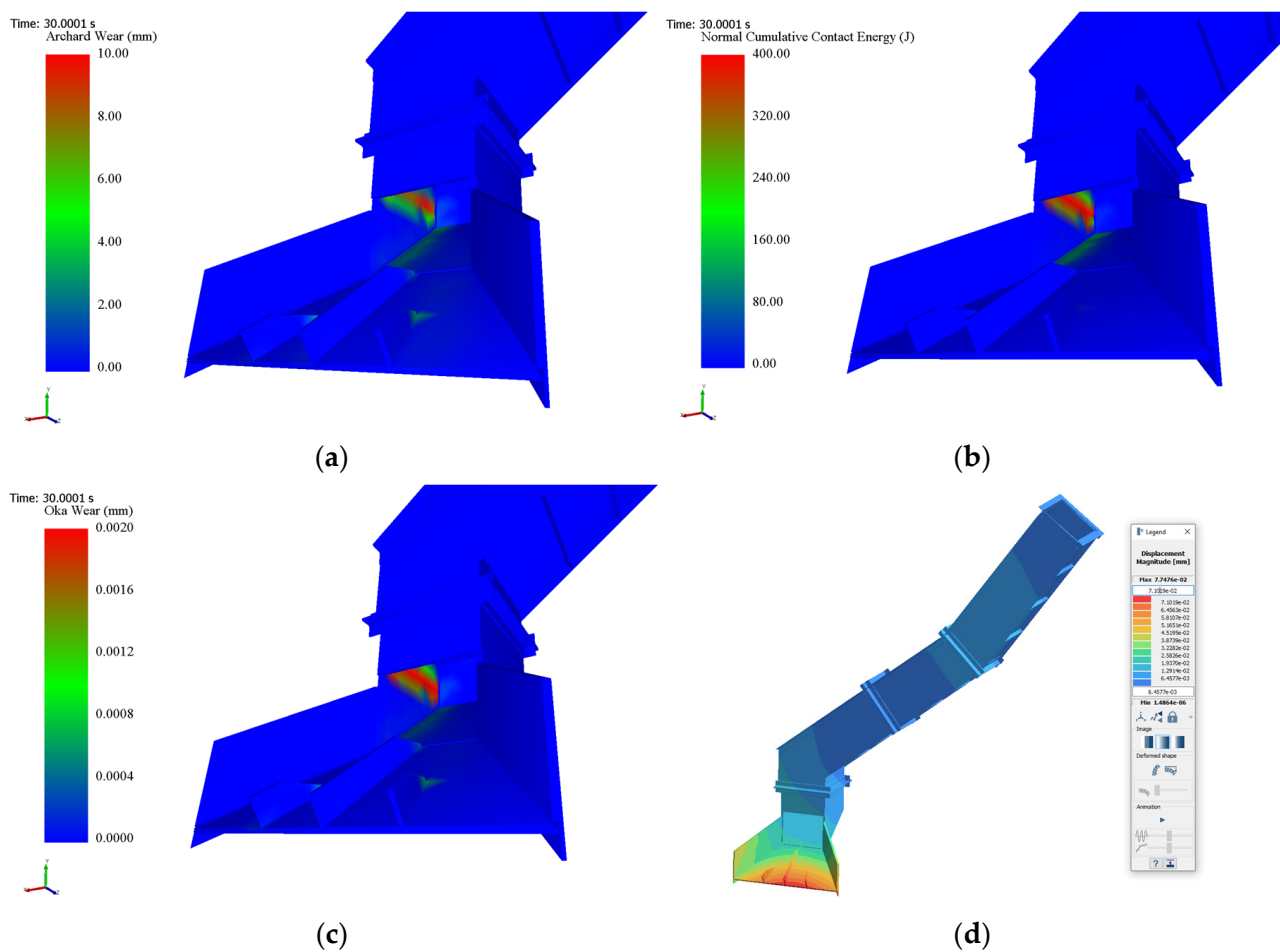


Figure 12. Calculation results for the side chute design: abrasive wear on the chute surface (a); accumulated contact energy on the chute surface in the normal direction (b); erosive wear on the chute surface (c); displacements map—MFree method (d).

To obtain the strength analysis results, the field of force vectors that represent the interaction of each particle on the chute structure must be exported from the DEM-based software tool to FEM- or MFree-based software.

3.3. Coke Classification Line

Two variants of the coke classification line were created. The first line variant was intended for classifying the material according to aggregate size. It consisted of a feed chute, a trapezoidal feeder and a vibrating screen (Figure 13a). Both the trapezoidal feeder and the screen were subjected to forced vibrations. This was possible due to their elastic mounting. The forcing was realized by rotating counter-rotating masses that cause centrifugal forces. These forces cancel out and add up at specific positions, which excites a feeder and a screen. The harmonic motion of a linear trajectory is the result of exciting the feeder and screen. The movement parameters and types of screens are selected depending on the process requirements, based on the following parameters: angle of inclination of the screen surface to the ground; frequency, amplitude, and direction of vibrations and the size of the sieve mesh. In the second variant, a combination of DEM computational models with software based on the CFD method in co-simulation mode was used. Instead of a screen, a tank with liquid, which enabled the classification of bulk materials with different densities, was used (Figure 13b).

The following boundary conditions were defined: vibration characteristics of the feeder—vibration frequency: 975 min^{-1} , vibration amplitude: 4.5 mm; vibration character-

istics of the screen—vibration frequency: 730 min^{-1} , vibration amplitude: 7 mm; angles of inclination of the linear vibration trajectory of the feeder and screener from the horizontal: 42° , 32° ; sieve mesh dimension: $60 \times 60 \text{ mm}$; line for classification according to aggregate size—feed rate: 720 t/h ; line for classifying the bulk material of different densities—feed size: 54 t/h (material of density of 550 kg/m^3), 54 t/h (material of density 2000 kg/m^3); liquid density: 1000 kg/m^3 , forced liquid flow: 0.5 m/s . Figure 14 shows the selected DEM simulation results for the lines to be classified according to aggregate size. In turn, Figure 15 shows the results for the lines for classifying bulk materials of different densities.

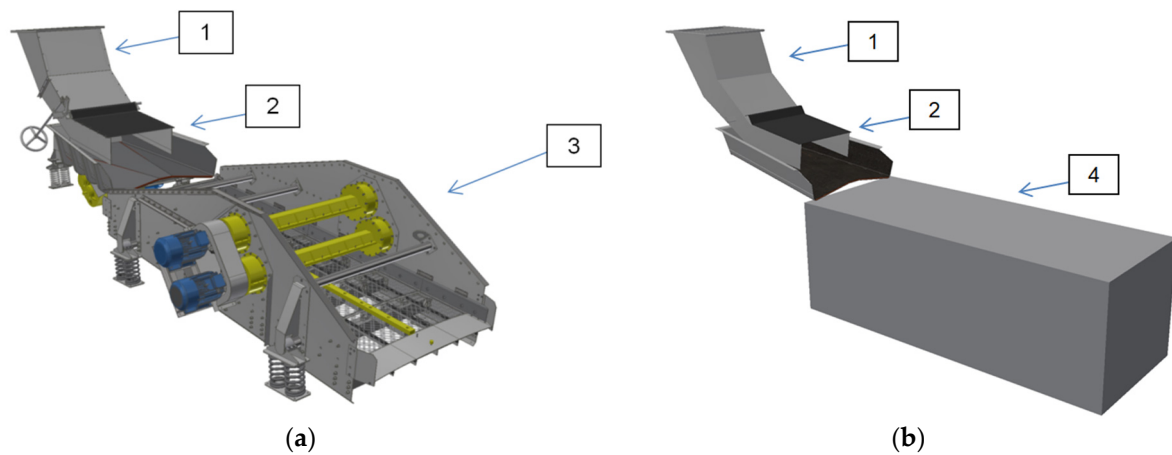


Figure 13. Fragment of the coke classification lines for the blast furnace, sorting particles by their size (a) and density (b): chute (1), trapezoidal feeder (2), vibrating screen (3), liquid tank (4).

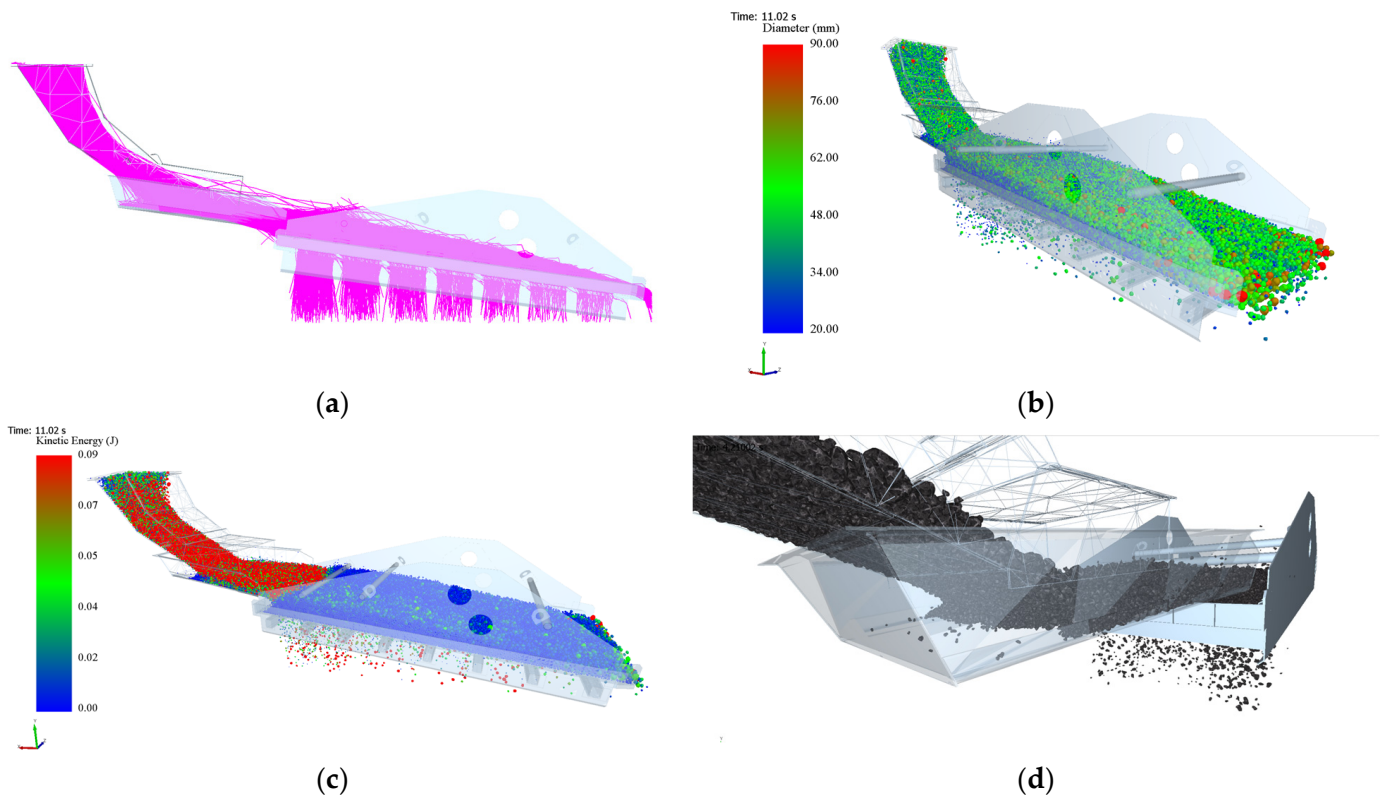


Figure 14. Calculation results for classification line according to aggregate size: direction of particle movement—the so-called stream (a), particle diameter (b), kinetic energy of particles (c), general view of moving particles on the classifying line—use of the so-called template (d).

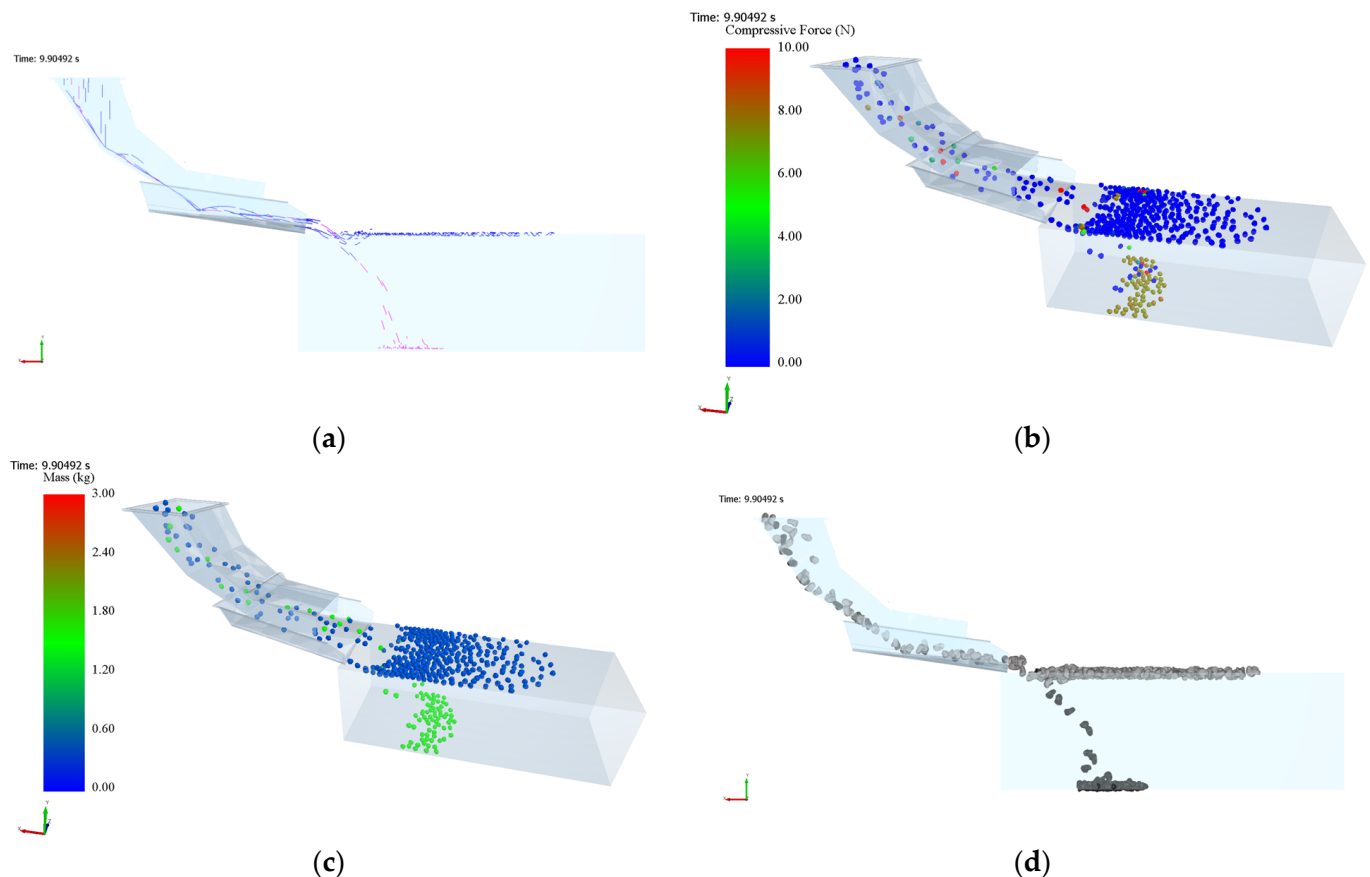


Figure 15. Calculation results for the line classifying the bulk material of different densities: stream (a), compressive forces acting on the particles (b), particle mass (c), general view of moving particles on the classifying line-use of the so-called template (d).

4. Conclusions

The main physical parameters necessary to develop computational models of aggregates in a software environment based on the discrete element method include the bulk density, angle of natural repose, internal friction coefficient, and external friction coefficient. Data from field tests enable creating computational models for bulk materials of similar physical parameters. The computational models obtained in this way are a part of larger computational tasks, where the bulk material is the source of the load to selected machine components that are mostly exposed to impacts and displacements of a bulk material in the technological or transport process.

Depending on the type of process to be analyzed, the types of numerical analyses have to be determined. For processes such as the screening of bulk materials (without the use of liquids), only DEM-type analyses are sufficient. For analyses in which the most important aspect is the analysis of fluid flow (analysis of valve performance, cooling systems), CFD-type analyses are sufficient. On the other hand, consideration of phenomena of combining the two, such as the analysis of phenomena occurring in scrubbers or material classifiers, even with the use of heavy fluid, requires the use of combined CFD+DEM analyses.

Figure 16 shows a generalized diagram of how the proposed numerical analyses approach can be applied to the machinery life cycle.

By analyzing the phenomena occurring in individual processes, it is possible to modify and manage the product life cycle. Using numerical analyses, it is possible to determine the areas at risk of increased wear. Wear can be predicted, and consequently, breaks can be planned for the maintenance, repair, or replacement of individual components. In the case of new machines, it is possible to use the results of the numerical analyses to select different materials for different areas of the machine. Differentiating both the type of material and

geometric features (e.g., wall thickness) will allow both the failure-free operation of the machine to be prolonged (by reinforcing the critical areas most exposed to wear) and an economical approach to design by saving material in areas that are not subject to rapid wear. As a result, the application of the proposed handling algorithm enables more accurate life cycle planning than was previously possible, thus ensuring that both the environment and the machine user's satisfaction and production costs are taken care of.

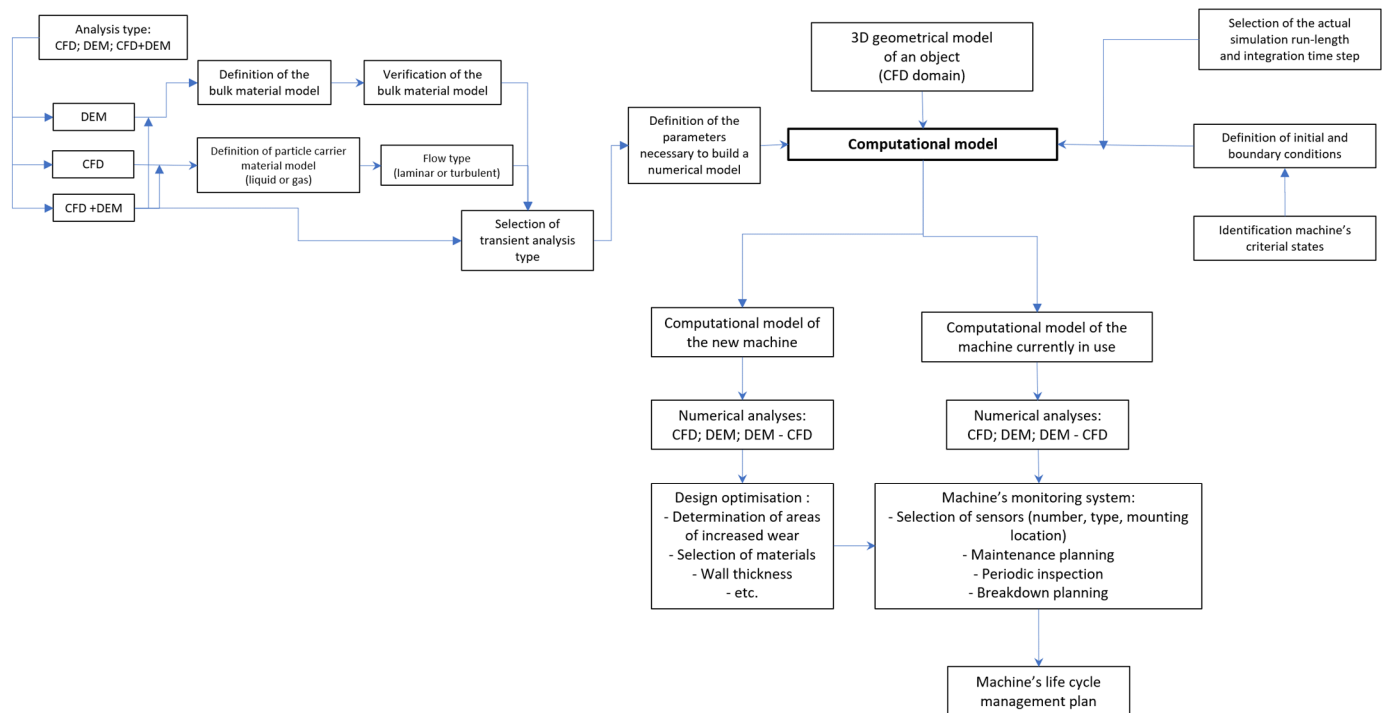


Figure 16. Generalized diagram of the usage of the proposed numerical analyses.

The use of DEM to simulate the operation of coke classification enables an assessment of its effectiveness and efficiency based on the selected geometric features (e.g., arrangement and size of the meshes on the screen) and other physical parameters (e.g., direction, amplitude, and frequency of vibrations of some components). An analysis of the calculation results enables easier determine the directions for optimizing both geometric features and the required material parameters of each device. In turn, combining the computer fluid mechanics method and the discrete element method to simulate multi-physical phenomena extends the use of virtual prototyping of the machines and devices used in extracting and processing the bulk materials, also assuming that, e.g., fluids are used in the technological process. These include using pulsating jigs or devices to extract deposits from the bottom of water reservoirs.

Numerical simulations using DEM require fewer financial expenses than stand tests, and the results are obtained faster than in the case of stand tests. At the designing stage, it is possible to assess the impact of changes in the geometric form of a machine, assembly, or part on the rate of their wear. The use of DEM to identify loads resulting from the movement of bulk material enables assessing the strength of the structure, including the impact of the type of material from which it will be made. In this article, the results are presented for the particles (linear and angular velocities, compressive forces, diameters, kinetic energy, and mass) and for the bulk material preparation device (abrasive and erosive wear, accumulated contact energy, displacements). The disadvantages include a low calculation accuracy, resulting from the need to empirically define material constants that are required in wear models (e.g., in the abrasive wear model according to Archard).

Including the presented numerical methods when designing the processes of new machines and devices improves their implementation in terms of timeliness and contributes

to minimizing the risk of making substantive errors. Moreover, the energy intensity of the designed machine can be assessed and reduced as well, which has significant economic consequences at the stage of its future operation.

Author Contributions: Conceptualization, J.T.; methodology, J.T.; validation, D.K., K.S. and P.M.; data curation, D.K.; writing—original draft preparation, J.T. and K.S.; writing—review and editing, J.T., K.S. and D.K. All authors have read and agreed to the published version of the manuscript.

Funding: The APC was funded by KOMAG Institute of Mining Technology.

Institutional Review Board Statement: Not applicable.

Informed Consent Statement: Not applicable.

Data Availability Statement: The datasets presented in this article are not readily available because they are the results of the KOMAG Institute’s internal research work, which are financed from statutory funds and as such can only be used for the Institute’s own use. Requests to access the datasets should be directed to info@komag.eu e-mail address.

Acknowledgments: Calculations were carried out at the Academic Computer Centre in Gdańsk, Poland.

Conflicts of Interest: The authors declare no conflicts of interest.

References

- Available online: <https://www.flyability.com/mining-industry> (accessed on 20 April 2024).
- Available online: <https://businesswithoutlimits.pl/jakie-sa-galezie-przemyslu/> (accessed on 20 April 2024).
- Available online: https://www.brainkart.com/article/Mineral-Resources_41102/ (accessed on 20 April 2024).
- Matusiak, P.; Kowol, D.; Suponik, T.; Franke, D.M.; Nuckowski, P.M.; Tora, B.; Pomykała, R. Selective Crushing of Run-of-Mine as an Important Part of the Hard Coal Beneficiation Process. *Energies* **2021**, *14*, 3167. [CrossRef]
- Available online: <https://www.statista.com/statistics/589945/iron-ore-production-gross-weight-worldwide/> (accessed on 20 April 2024).
- Available online: <https://www.globaldata.com/store/report/iron-ore-mining-market-analysis/> (accessed on 20 April 2024).
- Available online: <https://www.statista.com/statistics/1003518/global-manganese-production-volume/> (accessed on 20 April 2024).
- Available online: <https://www.theguardian.com/environment/2022/apr/26/50bn-tonnes-of-sand-and-gravel-extracted-each-year-finds-un-study> (accessed on 20 April 2024).
- Available online: <https://www.foruimining.com/solutions/screening-machine-commonly-used-in-iron-ore-production-line/> (accessed on 20 April 2024).
- Available online: <https://www.multotec.com/en/iron-ore-screening> (accessed on 20 April 2024).
- Available online: <https://derrick.com/2015/06/10/iron-ore/> (accessed on 20 April 2024).
- Available online: <https://www.cdegroupp.com/products/screening> (accessed on 20 April 2024).
- Available online: <https://www.powerscreen.com/en/equipment/screening/horizontal-screens> (accessed on 20 April 2024).
- Available online: <https://www.kemperequipment.com/screening-equipment.php> (accessed on 20 April 2024).
- Friebe, P.; Baron, R.; Sheketa, V. Concept of a CDR Resonance Screen. *Min. Mach.* **2022**, *40*, 8–18.
- Qingliang, G.; Gu, G. Application of Flip Flow Screen in Sihe Coal Preparation Plant. In *XVIII International Coal Preparation Congress*; Litvinenko, V., Ed.; Springer International Publishing: Cham, Switzerland, 2016; pp. 913–918.
- Lu, J.; Duan, C.; Pan, M.; Jiang, H.; Huang, L.; Guo, P.; Dombon, E. Evaluation of Coal Screening Performance by Spatial Image Reconstruction Method. *Fuel* **2023**, *337*, 126881. [CrossRef]
- Available online: <https://www.rhewum.com/en/applications-screening-machines/salt> (accessed on 20 April 2024).
- Venugopal, R.; Patel, J.P.; Bhar, C. Coal Washing Scenario in India and Future Prospects. *Int. J. Coal Sci. Technol.* **2016**, *3*, 191–197. [CrossRef]
- Lutyński, A. KOMAG Activities in the Domestic and International Research Areas. *Min. Mach.* **2021**, *39*, 47–60.
- Matusiak, P.; Kowol, D. Use of State-of-the-Art Jigs of KOMAG Type for a Beneficiation of Coking Coal. *Min. Mach.* **2020**, *161*, 46–55.
- Cierpisz, S.; Kryca, M.; Sobierajski, W. Control of Coal Separation in a Jig Using a Radiometric Meter. *Miner. Eng.* **2016**, *95*, 59–65. [CrossRef]
- Tripathy, A.; Panda, L.; Sahoo, A.K.; Biswal, S.K.; Dwari, R.K.; Sahu, A.K. Statistical Optimization Study of Jigging Process on Beneficiation of Fine Size High Ash Indian Non-Coking Coal. *Adv. Powder Technol.* **2016**, *27*, 1219–1224. [CrossRef]
- Kowol, D.; Matusiak, P. Use of a Jig Beneficiation Process for Obtaining Mineral Raw Materials. *IOP Conf. Ser. Mater. Sci. Eng.* **2019**, *545*, 012006. [CrossRef]

25. Gschwenter, V.L.S.; Tubino, R.M.C.; Ambrós, W.M.; Miltzarek, G.L.; Sampaio, C.H.; Moncunill, J.O.; Cazacliu, B.G.; Dal Molin, D.C.C. Production of High-Quality Coarse Recycled Aggregates through a Two-Stage Jigging Process. *Minerals* **2022**, *12*, 532. [CrossRef]
26. Ramam, D.B.S. Jigging in Iron Ore Beneficiation: Process Parameter Optimization to Improve Consistency in Product Quality. In Proceedings of the International Mineral Processing Congress, New Delhi, India, 24–28 September 2012; Available online: <https://onemine.org/documents/jigging-in-iron-ore-beneficiation-process-parameter-optimization-to-improve-consistency-in-product-quality> (accessed on 16 April 2024).
27. Shukla, V.; Kumar, C.R.; Chakraborty, D.P.; Kumar, A. Optimization of Jigging Process Parameters to Beneficiate Iron Ore Fines—A Case Study of Tatasteel. *Inżynieria Miner. J. Pol. Miner. Eng. Soc.* **2019**, *21*, 165–170.
28. Myburgh, H.A.; Nortje, A. Operation and Performance of the Sishen Jig Plant. *J. South. Afr. Inst. Min. Metall.* **2014**, *114*, 569–574.
29. Das, B.; Prakash, S.; Das, S.K.; Reddy, P.S.R. Effective Beneficiation of Low Grade Iron Ore Through Jigging Operation. *JMMCE* **2008**, *7*, 27–37. [CrossRef]
30. Sivrikaya, Q.; Arol, A.I. Investigation of Beneficiation of a Manganese Ore by Jig. In Proceedings of the XVII Balkan Mineral Processing Congress, Antalya, Turkey, 1 November 2017.
31. Rousseau, M.; Blancher, S.B.; Contessotto, R.; Wallmach, T. Beneficiation of Low Grade Manganese Ore by Jigging in a Specially Designed Ore Dressing Unit. In Proceedings of the XXVIII International Mineral Processing Congress Proceedings, Quebec City, QC, Canada, 15 September 2016.
32. Ambrós, W.M. Jigging: A Review of Fundamentals and Future Directions. *Minerals* **2020**, *10*, 998. [CrossRef]
33. Xiangjun, Q. DEM Simulations in Mining and Mineral Processing. In Proceedings of the 7th International Conference on Discrete Element Methods, Dalian, China, 4 August 2016.
34. Dong, K.J.; Yu, A.B.; Brake, I. DEM Simulation of Particle Flow on a Multi-Deck Banana Screen. *Miner. Eng.* **2009**, *22*, 910–920. [CrossRef]
35. Jahani, M.; Farzanegan, A.; Noaparast, M. Investigation of Screening Performance of Banana Screens Using LIGGGHTS DEM Solver. *Powder Technol.* **2015**, *283*, 32–47. [CrossRef]
36. Chen, Y.; Tong, X. Application of the DEM to Screening Process: A 3D Simulation. *Min. Sci. Technol.* **2009**, *19*, 493–497. [CrossRef]
37. Cheng, J.; Ren, T.; Zhang, Z.; Liu, D.; Jin, X. A Dynamic Model of Inertia Cone Crusher Using the Discrete Element Method and Multi-Body Dynamics Coupling. *Minerals* **2020**, *10*, 862. [CrossRef]
38. Larsson, S.; Rodríguez Prieto, J.M.; Heiskari, H.; Jonsén, P. A Novel Particle-Based Approach for Modeling a Wet Vertical Stirred Media Mill. *Minerals* **2021**, *11*, 55. [CrossRef]
39. Rodríguez, V.A.; Barrios, G.K.P.; Bueno, G.; Tavares, L.M. Investigation of Lateral Confinement, Roller Aspect Ratio and Wear Condition on HPGR Performance Using DEM-MBD-PRM Simulations. *Minerals* **2021**, *11*, 801. [CrossRef]
40. Klichowicz, M.; Lieberwirth, H. Grain-Based DEM for Particle Bed Comminution. *Minerals* **2021**, *11*, 306. [CrossRef]
41. Doroszuk, B.; Król, R. Industry Scale Optimization: Hammer Crusher and DEM Simulations. *Minerals* **2022**, *12*, 244. [CrossRef]
42. Moncada, M.; Toledo, P.; Betancourt, F.; Rodríguez, C.G. Torque Analysis of a Gyratory Crusher with the Discrete Element Method. *Minerals* **2021**, *11*, 878. [CrossRef]
43. Mendyka, P.; Kasza, P.; Feliks, J.; Stopka, G. Modeling of Granulation Process in Plate Granulator Using Dem. In Proceedings of the International Multidisciplinary Scientific Geoconference: Science and Technologies in Geology, Exploration and Mining, Geology & Mineral Processing, Albena, Bulgaria, 5 July 2017; Volume 17.
44. Svanberg, A.; Larsson, S.; Mäki, R.; Jonsén, P. Full-Scale Simulation and Validation of Wear for a Mining Rope Shovel Bucket. *Minerals* **2021**, *11*, 623. [CrossRef]
45. Gospodarczyk, P. Modeling and Simulation of Coal Loading by Cutting Drum in Flat Seams. *AMS* **2016**, *61*, 365–379. [CrossRef]
46. Li, X.; Wang, S.; Malekian, R.; Hao, S.; Li, Z. Numerical Simulation of Rock Breakage Modes under Confining Pressures in Deep Mining: An Experimental Investigation. *IEEE Access* **2016**, *4*, 5710–5720. [CrossRef]
47. Liu, Q.-M.; Li, W.-P.; Li, X.-Q.; Hu, G. Study on Deformation Characteristics of Coal Roof Overlapping Mining under the Coverage of Magmatic Rocks with DEM Simulation. *Procedia Eng.* **2011**, *26*, 101–106. [CrossRef]
48. Hussain, C.M.; Paulraj, M.S.; Nuzhat, S. *Source Reduction and Waste Minimization*; Elsevier: Amsterdam, The Netherlands, 2022.
49. Cundall, P.A. A Computer Model for Simulating Progressive Large Scale Movements in Blocky Rock Systems. In Proceedings of the Symposium of the International Society of Rock Mechanics, Nancy, France, 6 October 1971; Volume 1.
50. Cundall, P.A.; Hart, R.D. Numerical Modelling of Discontinua. *Eng. Comput.* **1992**, *9*, 101–113. [CrossRef]
51. Altair EDEM User's Manual. 2022. Available online: https://2022.help.altair.com/2022.1/EDEM/index.htm#t=Getting_Started.htm#Getting_Started (accessed on 18 April 2024).
52. Hertz, H. On the Contact of Elastic Solids. *J. Fur Die Reine Und Angew. Math.* **1882**, *92*, 156–171. [CrossRef]
53. Mindlin, R.D. Compliance of Elastic Bodies in Contact. *J. Appl. Mech.* **1949**, *16*, 259–268. [CrossRef]
54. Mindlin, R.D.; Deresiewicz, H. Elastic Spheres in Contact under Varying Oblique Force. *J. Appl. Mech.* **1953**, *20*, 327–344. [CrossRef]
55. Tsuji, Y.; Tanaka, T.; Ishida, T. Lagrangian Numerical Simulation of Plug Flow of Cohesionless Particles in a Horizontal Pipe. *Powder Technol.* **1992**, *71*, 239–250. [CrossRef]
56. Cundall, P.A.; Strack, O.D.L. A Discrete Numerical Model for Granular Assemblies. *Géotechnique* **1979**, *29*, 47–65. [CrossRef]

57. Sakaguchi, H.; Ozaki, E.; Igarashi, T. Plugging of the Flow of Granular Materials during the Discharge from a Silo. *Int. J. Mod. Phys. B* **1993**, *7*, 1949–1963. [[CrossRef](#)]
58. Johnson, K.L.; Kendall, K.; Roberts, A.D. Surface Energy and the Contact of Elastic Solids. *Proc. R. Soc. Lond. A* **1971**, *324*, 301–313.
59. Walton, O.R.; Braun, R.L. Viscosity, Granular-temperature, and Stress Calculations for Shearing Assemblies of Inelastic, Frictional Disks. *J. Rheol.* **1986**, *30*, 949–980. [[CrossRef](#)]
60. Walton, O.R.; Braun, R.L. Stress Calculations for Assemblies of Inelastic Spheres in Uniform Shear. *Acta Mech.* **1986**, *63*, 73–86. [[CrossRef](#)]
61. Jones, R. From Single Particle AFM Studies of Adhesion and Friction to Bulk Flow: Forging the Links. *Granul. Matter* **2003**, *4*, 191–204. [[CrossRef](#)]
62. Jones, R.; Pollock, H.M.; Geldart, D.; Verlinden-Luts, A. Frictional Forces between Cohesive Powder Particles Studied by AFM. *Ultramicroscopy* **2004**, *100*, 59–78. [[CrossRef](#)]
63. Archard, J.F. Contact and Rubbing of Flat Surfaces. *J. Appl. Phys.* **1953**, *24*, 981–988. [[CrossRef](#)]
64. Oka, Y.I.; Okamura, K.; Yoshida, T. Practical Estimation of Erosion Damage Caused by Solid Particle Impact: Part 1: Effects of Impact Parameters on a Predictive Equation. *Wear* **2005**, *259*, 95–101. [[CrossRef](#)]
65. Oka, Y.I.; Yoshida, T. Practical Estimation of Erosion Damage Caused by Solid Particle Impact: Part 2: Mechanical Properties of Materials Directly Associated with Erosion Damage. *Wear* **2005**, *259*, 102–109. [[CrossRef](#)]

Disclaimer/Publisher’s Note: The statements, opinions and data contained in all publications are solely those of the individual author(s) and contributor(s) and not of MDPI and/or the editor(s). MDPI and/or the editor(s) disclaim responsibility for any injury to people or property resulting from any ideas, methods, instructions or products referred to in the content.